ELSEVIER

Fluid Phase Equilibria 161 (1999) 135–151

FLUID PHASE EQUILIBRIA

# Wax content measurements in partially frozen paraffinic systems

C. Dauphin [a], J.L. Daridon [a,*], J. Coutinho [b], P. Baylère [c], M. Potin-Gautier [c]

[a] *Laboratoire Haute Pression, Centre Universitaire de Recherche Scientifique, Université de Pau, Avenue de l'Université, 64000 Pau, France*

[b] *Departamento de Quimica da Universidade de Aveiro, 3810 Aveiro, Portugal*

[c] *Laboratoire de Chimie Analytique, Centre Universitaire de Recherche Scientifique, Université de Pau, Avenue de l'Université, 64000 Pau, France*

Received 6 October 1998; accepted 28 January 1999

**Abstract**

Waxy solid content and wax composition were measured as a function of temperature below the onset crystallization temperatures in several synthetic systems made up of a solvent (decane) and a paraffinic heavy fraction. The heavy fraction of the first system studied was made up of a regular series of heavy alkanes ranging from $C_{18}$ to $C_{36}$. Whereas in other systems, some intermediate paraffins were removed from the series in order to have various «bimodal» distributions. Experimental data were used to test the capacity of a local composition model to predict solid phase behaviors of these bimodal paraffinic distributions. 

*Keywords:* Solid–liquid equilibrium; Wax; Paraffin

## 1. Introduction

In cold regions, the *n*-paraffin content greatly affects flow properties of crude oil in production tubing or in transportation pipelines when temperature falls below the wax appearance temperature. Some heavy oils are so waxy that *n*-paraffins solid deposits clog up filters and obstruct pipelines. In order to prevent the plugging of tubing and to improve the flow property of such oils, two distinct methods are widely employed: a chemical technique, which rests on addition of wax inhibitors or

* Corresponding author. Tel.: +33-5-59-92-30-54; fax: +33-5-59-80-83-82; e-mail: jean-luc.daridon@univ-pau.fr

0378-3812/99/$ - see front matter 
PII: S0378-3812(99)00155-7

flow improvers, and a thermodynamic technique. Wax appearance which is linked to changing temperature and fluid composition caused by bringing the well into production, can be altered by heating or by diluting with light crude oils. Design and simulation of such removal thermodynamic process requires thermodynamic models which are able to adequately simulate liquid–solid phase equilibria of multi-paraffins systems. In a previous work [1], it has been seen that a solid solution model [2,3] in which the solid state is described by Wilson equation [4] leads to a satisfactory representation of narrow paraffin distribution. However, when paraffin distributions widen out [5], the nonideality of solutions increase and the model over-estimates the precipitation of the lightest components. To overcome this problem, assuming that the high nonideality between the heaviest and the lightest paraffins leads to the coexistence of several solid solutions, Coutinho [6] has propose to use the UNIQUAC model [7], which allows solid phase splits, instead of Wilson equation.

In order to check the predictive capacity of this model for complex waxy distributions, measurements of liquid–solid equilibria were performed on several systems made up of a solvent (decane) and a bimodal paraffin distribution. The heavy fraction of the first system studied was made up of a regular series of heavy alkanes ranging from $C_{18}$ to $C_{36}$. Whereas in other systems, some intermediate paraffins were removed from the series in order to have various bimodal distribution heavy fractions. Measurements were carried out in a transparent filtration cell to determined the cloud point as well as the composition and the quantity of the solid deposits vs. temperature. Experimental results were then compared with those predicted by the solid solution model developed by Coutinho et al. [3] using either UNIQUAC or Wilson local composition models.

## 2. Measurements

Measurements were carried out on various systems made up of a solvent (decane) plus a synthetic wax in the global proportion of 4 moles of decane to 1 mole of wax. The composition of waxes is the sole difference from one system to the other. They are essentially made up of heavy *n*-paraffins whose chain length range from 18 to 36.

The first system studied (*BIM 0*) is composed of the full series of *n*-paraffin within which the proportion of *n*-paraffins is regularly decreasing from $C_{18}$ to $C_{36}$ according to the following recurrence relationship

$$x_{C_{n+1}} = \alpha x_{C_n}, \tag{1}$$

where the coefficient $\alpha$ was fixed at 0.885 in such a way as to match the average compositions observed in waxy crude oils and thus correspond to a simplified representation of the heavy fraction of reservoir fluids.

In other systems, 3 and then 5, 9 and 13 intermediate paraffins were removed from the full series in order to break down the continual distribution into two separate series (bimodal distribution). The proportion of paraffins between them is still described by Eq. (1) with the same value of $\alpha$. Table 1 presents the various systems investigated along with their global composition (mass %). The origin of pure *n*-alkanes components as well as their state purity are also given in Table 1. The components were used without further purification after having checked the purity by GC chromatography.

Table 1
Feed composition (mass %) of the systems

| | *Bim 0* | *Bim 3* | *Bim 5* | *Bim 9* | *Bim 13* | References | Purity |
|---|---|---|---|---|---|---|---|
| *n*-$C_{10}$ | 63.84 | 64.25 | 64.65 | 65.59 | 66.65 | Aldrich | > 99.0 |
| *n*-$C_{18}$ | 4.276 | 4.872 | 5.383 | 6.958 | 10.57 | Fluka | > 99.0 |
| *n*-$C_{19}$ | 3.871 | 4.411 | 4.874 | 6.301 | 9.571 | Aldrich | 99.0 |
| *n*-$C_{20}$ | 3.494 | 3.981 | 4.400 | 5.688 | 8.641 | Aldrich | 99.0 |
| *n*-$C_{21}$ | 3.149 | 3.587 | 3.963 | 5.124 | – | Fluka | > 98.0 |
| *n*-$C_{22}$ | 2.828 | 3.221 | 3.561 | 4.603 | – | Aldrich | 99.0 |
| *n*-$C_{23}$ | 2.536 | 2.889 | 3.193 | – | – | Aldrich | 99.0 |
| *n*-$C_{24}$ | 2.270 | 2.586 | 2.858 | – | – | Fluka | > 99.0 |
| *n*-$C_{25}$ | 2.028 | 2.310 | – | – | – | Fluka | > 98.0 |
| *n*-$C_{26}$ | 1.811 | – | – | – | – | Aldrich | > 99.0 |
| *n*-$C_{27}$ | 1.612 | – | – | – | – | Fluka | > 98.0 |
| *n*-$C_{28}$ | 1.441 | – | – | – | – | Fluka | > 98.0 |
| *n*-$C_{29}$ | 1.274 | 1.451 | – | – | – | Fluka | > 99.5 |
| *n*-$C_{30}$ | 1.130 | 1.290 | 1.424 | – | – | Aldrich | > 99.0 |
| *n*-$C_{31}$ | 1.004 | 1.142 | 1.262 | – | – | Kasei | > 97.0 |
| *n*-$C_{32}$ | 0.887 | 1.011 | 1.119 | 1.444 | – | Kasei | > 98.0 |
| *n*-$C_{33}$ | 0.788 | 0.895 | 0.989 | 1.280 | – | Fluka | > 99.5 |
| *n*-$C_{34}$ | 0.695 | 0.790 | 0.873 | 1.129 | 1.716 | Kasei | > 98.0 |
| *n*-$C_{35}$ | 0.522 | 0.698 | 0.771 | 0.998 | 1.516 | Fluka | > 99.5 |
| *n*-$C_{36}$ | 0.541 | 0.616 | 0.682 | 0.881 | 1.337 | Kasei | > 98.0 |
| Mw/g $mol^{-1}$ (heavy part) | 323.64 | 316.73 | 311.27 | 298.90 | 284.92 | | |

Cloud point temperatures were determined optically by measuring the temperature of disappearance of the last crystal of a two-phase system slowly heated and continuously stirred in a glass vessel [8]. The measured crystallization temperatures are listed in Table 2.

The characterization of the solid deposit as a function of temperature was carried out every 5 or 10 K below the onset crystallization temperature by phase separation. The experimental apparatus, which has been described in a previous publication, is composed essentially of a transparent filtration cell [5]. In this cell, after 1 day of equilibrium at the desired temperature, a liquid part was separate by compression of the partially frozen system through a filter of porosity 4 μm. The filtrate liquid as well as the solid residue, which corresponds to the superposition of the solid part and an entrapped liquid part, were then weighed and analyzed in A HP 6890 Gas Chromatograph using a OV-5 30 m column with a temperature program of 3°C/min from 50°C to 320°C. The proportion $Y$ of trapped

Table 2
Deviations ($K$) between experimental and calculated onset crystallization temperatures

| | *Bim 0* | *Bim 3* | *Bim 5* | *Bim 9* | *Bim 13* |
|---|---|---|---|---|---|
| Tex $p/K$ | 308.75 | 309.65 | 310.37 | 311.33 | 312.81 |
| Wilson | 0.7 | 0 | 0 | −0.3 | −0.7 |
| UNIQUAC | −1.7 | −2.1 | −1.9 | −1.7 | −1.4 |

Table 3
Experimental characterization of the partially frozen system *BIM 0* as a function of temperature below the onset crystallization temperature

| | 303.15 K | 298.15 K | 293.25 K | 288.05 K | 283.25 K | 273.15 K | 263.15 K |
|---|---|---|---|---|---|---|---|
| *Waxy solid content (mass %)* | | | | | | | |
| | 2.33 | 5.09 | 7.15 | 11.83 | 15.26 | 22.76 | 29.51 |
| *Solid composition (mass %)* | | | | | | | |
| $C_{18}$ | 0.00 | 0.00 | 0.00 | 0.00 | 0.05 | 0.90 | 3.51 |
| $C_{19}$ | 0.00 | 0.00 | 0.00 | 0.00 | 0.24 | 2.46 | 6.77 |
| $C_{20}$ | 0.00 | 0.00 | 0.00 | 0.15 | 0.77 | 4.97 | 8.95 |
| $C_{21}$ | 0.00 | 0.07 | 0.09 | 0.53 | 1.96 | 7.40 | 9.36 |
| $C_{22}$ | 0.00 | 0.11 | 0.31 | 1.44 | 4.00 | 8.83 | 8.94 |
| $C_{23}$ | 0.00 | 0.17 | 0.81 | 3.06 | 6.31 | 9.02 | 8.15 |
| $C_{24}$ | 0.12 | 0.41 | 1.98 | 5.39 | 8.25 | 8.77 | 7.52 |
| $C_{25}$ | 0.24 | 0.98 | 3.88 | 7.58 | 9.12 | 8.09 | 6.78 |
| $C_{26}$ | 0.58 | 2.19 | 6.38 | 9.17 | 9.33 | 7.48 | 6.17 |
| $C_{27}$ | 1.37 | 4.15 | 8.48 | 9.66 | 8.86 | 6.68 | 5.46 |
| $C_{28}$ | 3.00 | 6.81 | 10.06 | 9.71 | 8.36 | 6.08 | 4.93 |
| $C_{29}$ | 5.52 | 9.43 | 10.66 | 9.25 | 7.67 | 5.44 | 4.38 |
| $C_{30}$ | 8.59 | 11.30 | 10.55 | 8.56 | 6.95 | 4.84 | 3.88 |
| $C_{31}$ | 11.24 | 11.91 | 9.76 | 7.61 | 6.09 | 4.19 | 3.35 |
| $C_{32}$ | 13.73 | 12.28 | 9.26 | 7.05 | 5.61 | 3.81 | 3.04 |
| $C_{33}$ | 14.98 | 11.89 | 8.54 | 6.44 | 5.10 | 3.46 | 2.75 |
| $C_{34}$ | 15.03 | 10.95 | 7.58 | 5.66 | 4.47 | 3.01 | 2.40 |
| $C_{35}$ | 12.29 | 8.49 | 5.73 | 4.29 | 3.38 | 2.26 | 1.80 |
| $C_{36}$ | 13.31 | 8.87 | 5.92 | 4.43 | 3.48 | 2.32 | 1.86 |
| *Liquid composition (mass %)* | | | | | | | |
| $C_{10}$ | 66.10 | 69.30 | 70.50 | 72.41 | 76.29 | 83.54 | 90.14 |
| $C_{18}$ | 4.33 | 4.29 | 4.54 | 4.90 | 4.87 | 5.08 | 4.50 |
| $C_{19}$ | 3.93 | 3.88 | 4.11 | 4.42 | 4.38 | 4.14 | 2.66 |
| $C_{20}$ | 3.55 | 3.49 | 3.71 | 3.95 | 3.85 | 2.94 | 1.26 |
| $C_{21}$ | 3.20 | 3.14 | 3.33 | 3.49 | 3.24 | 1.82 | 0.60 |
| $C_{22}$ | 2.88 | 2.82 | 2.99 | 3.01 | 2.53 | 1.02 | 0.34 |
| $C_{23}$ | 2.56 | 2.49 | 2.60 | 2.43 | 1.76 | 0.57 | 0.20 |
| $C_{24}$ | 2.31 | 2.24 | 2.25 | 1.85 | 1.15 | 0.34 | 0.13 |
| $C_{25}$ | 2.05 | 1.96 | 1.81 | 1.27 | 0.71 | 0.21 | 0.08 |
| $C_{26}$ | 1.84 | 1.69 | 1.38 | 0.83 | 0.45 | 0.14 | 0.04 |
| $C_{27}$ | 1.59 | 1.37 | 0.96 | 0.52 | 0.28 | 0.08 | 0.03 |
| $C_{28}$ | 1.38 | 1.06 | 0.64 | 0.33 | 0.18 | 0.05 | 0.01 |
| $C_{29}$ | 1.14 | 0.76 | 0.41 | 0.21 | 0.11 | 0.03 | 0.01 |
| $C_{30}$ | 0.91 | 0.52 | 0.26 | 0.13 | 0.07 | 0.02 | 0.00 |
| $C_{31}$ | 0.67 | 0.33 | 0.16 | 0.08 | 0.04 | 0.01 | 0.00 |
| $C_{32}$ | 0.51 | 0.23 | 0.11 | 0.07 | 0.03 | 0.01 | 0.00 |
| $C_{33}$ | 0.39 | 0.16 | 0.09 | 0.05 | 0.02 | 0.01 | 0.00 |
| $C_{34}$ | 0.29 | 0.11 | 0.06 | 0.03 | 0.01 | 0.00 | 0.00 |
| $C_{35}$ | 0.19 | 0.07 | 0.04 | 0.02 | 0.01 | 0.00 | 0.00 |
| $C_{36}$ | 0.18 | 0.07 | 0.04 | 0.02 | 0.01 | 0.00 | 0.00 |

Table 4
Experimental characterization of the partially frozen system *BIM 3* as a function of temperature below the onset crystallization temperature

| | 305.15 K | 301.15 K | 296.05 K | 278.35 K | 273.15 K | 263.15 K |
|---|---|---|---|---|---|---|
| *Waxy solid content (mass %)* | | | | | | |
| | 2.51 | 4.17 | 5.64 | 16.64 | 22.43 | 28.30 |
| *Solid composition (mass %)* | | | | | | |
| $C_{18}$ | 0.00 | 0.00 | 0.00 | 0.65 | 1.56 | 4.78 |
| $C_{19}$ | 0.00 | 0.00 | 0.00 | 1.78 | 3.86 | 8.72 |
| $C_{20}$ | 0.00 | 0.00 | 0.00 | 4.11 | 7.13 | 10.95 |
| $C_{21}$ | 0.00 | 0.00 | 0.00 | 7.17 | 9.87 | 11.17 |
| $C_{22}$ | 0.00 | 0.00 | 0.00 | 9.84 | 11.16 | 10.59 |
| $C_{23}$ | 0.00 | 0.00 | 0.00 | 10.99 | 10.96 | 9.59 |
| $C_{24}$ | 0.00 | 0.00 | 0.22 | 11.05 | 10.30 | 8.68 |
| $C_{25}$ | 0.00 | 0.00 | 0.35 | 10.33 | 9.32 | 7.78 |
| $C_{29}$ | 4.22 | 6.15 | 9.59 | 7.64 | 6.38 | 5.07 |
| $C_{30}$ | 7.37 | 9.68 | 12.87 | 7.10 | 5.82 | 4.54 |
| $C_{31}$ | 10.92 | 12.82 | 14.57 | 6.44 | 5.23 | 4.04 |
| $C_{32}$ | 13.86 | 14.64 | 14.58 | 5.72 | 4.61 | 3.55 |
| $C_{33}$ | 15.88 | 15.31 | 13.85 | 5.11 | 4.12 | 3.15 |
| $C_{34}$ | 16.46 | 14.84 | 12.58 | 4.52 | 3.63 | 2.77 |
| $C_{35}$ | 16.16 | 13.92 | 11.34 | 4.01 | 3.22 | 2.45 |
| $C_{36}$ | 15.13 | 12.64 | 10.04 | 3.53 | 2.83 | 2.16 |
| *Liquid composition (mass %)* | | | | | | |
| $C_{10}$ | 65.12 | 66.75 | 67.35 | 77.10 | 81.91 | 89.41 |
| $C_{18}$ | 5.08 | 5.09 | 5.27 | 5.95 | 5.87 | 4.98 |
| $C_{19}$ | 4.63 | 4.65 | 4.81 | 5.17 | 4.67 | 2.81 |
| $C_{20}$ | 4.17 | 4.18 | 4.33 | 4.11 | 3.17 | 1.28 |
| $C_{21}$ | 3.74 | 3.75 | 3.88 | 2.91 | 1.85 | 0.61 |
| $C_{22}$ | 3.38 | 3.40 | 3.52 | 1.90 | 1.03 | 0.34 |
| $C_{23}$ | 3.00 | 3.01 | 3.10 | 1.18 | 0.61 | 0.22 |
| $C_{24}$ | 2.69 | 2.70 | 2.79 | 0.81 | 0.44 | 0.17 |
| $C_{25}$ | 2.40 | 2.41 | 2.47 | 0.61 | 0.34 | 0.14 |
| $C_{29}$ | 1.42 | 1.27 | 0.99 | 0.14 | 0.08 | 0.02 |
| $C_{30}$ | 1.17 | 0.95 | 0.62 | 0.07 | 0.03 | 0.01 |
| $C_{31}$ | 0.93 | 0.67 | 0.35 | 0.03 | 0.00 | 0.00 |
| $C_{32}$ | 0.71 | 0.44 | 0.20 | 0.01 | 0.00 | 0.00 |
| $C_{33}$ | 0.54 | 0.30 | 0.12 | 0.01 | 0.00 | 0.00 |
| $C_{34}$ | 0.42 | 0.20 | 0.08 | 0.00 | 0.00 | 0.00 |
| $C_{35}$ | 0.33 | 0.15 | 0.06 | 0.00 | 0.00 | 0.00 |
| $C_{36}$ | 0.27 | 0.11 | 0.05 | 0.00 | 0.00 | 0.00 |

liquid in the solid residue can be deduced from a mass balance for the solvent ($C_{10}$) which does not freeze in the experimental temperature range:

$$Y = \frac{X^{SR}_{C_{10}}}{X^{L}_{C_{10}}}. \quad (2)$$

Table 5
Experimental characterization of the partially frozen system *BIM 5* as a function of temperature below the onset crystallization temperature

| | 306.15 K | 298.15 K | 294.15 K | 286.25 K | 283.35 K | 273.45 K | 263.35 K |
|---|---|---|---|---|---|---|---|
| *Waxy solid content (mass %)* | | | | | | | |
| | 2.30 | 4.51 | 5.38 | 6.59 | 10.02 | 20.46 | 27.46 |
| *Solid composition (mass %)* | | | | | | | |
| $C_{18}$ | 0.00 | 0.00 | 0.00 | 0.02 | 0.22 | 2.05 | 6.11 |
| $C_{19}$ | 0.00 | 0.00 | 0.00 | 0.06 | 0.72 | 5.27 | 10.67 |
| $C_{20}$ | 0.00 | 0.00 | 0.00 | 0.15 | 2.06 | 9.40 | 12.84 |
| $C_{21}$ | 0.00 | 0.00 | 0.00 | 0.35 | 4.54 | 12.25 | 12.69 |
| $C_{22}$ | 0.00 | 0.00 | 0.00 | 0.67 | 7.59 | 13.23 | 11.89 |
| $C_{23}$ | 0.00 | 0.00 | 0.00 | 0.96 | 9.54 | 12.46 | 10.58 |
| $C_{24}$ | 0.00 | 0.00 | 0.00 | 1.15 | 9.98 | 11.36 | 9.51 |
| $C_{30}$ | 6.50 | 11.16 | 13.89 | 16.27 | 11.67 | 6.60 | 5.08 |
| $C_{31}$ | 10.47 | 14.76 | 16.37 | 16.94 | 11.58 | 6.08 | 4.59 |
| $C_{32}$ | 14.07 | 16.27 | 16.47 | 15.70 | 10.53 | 5.37 | 4.05 |
| $C_{33}$ | 16.60 | 16.17 | 15.43 | 14.09 | 9.36 | 4.74 | 3.56 |
| $C_{34}$ | 17.75 | 15.21 | 14.02 | 12.55 | 8.31 | 4.19 | 3.16 |
| $C_{35}$ | 17.72 | 13.90 | 12.58 | 11.16 | 7.37 | 3.71 | 2.80 |
| $C_{36}$ | 16.87 | 12.54 | 11.23 | 9.93 | 6.53 | 3.29 | 2.49 |
| *Liquid composition (mass %)* | | | | | | | |
| $C_{10}$ | 67.84 | 69.04 | 69.85 | 70.61 | 73.16 | 81.98 | 89.96 |
| $C_{18}$ | 5.23 | 5.46 | 5.47 | 5.53 | 5.75 | 6.07 | 4.97 |
| $C_{19}$ | 4.77 | 4.98 | 5.00 | 5.04 | 5.18 | 4.67 | 2.59 |
| $C_{20}$ | 4.29 | 4.50 | 4.51 | 4.54 | 4.51 | 3.04 | 1.11 |
| $C_{21}$ | 3.84 | 4.03 | 4.04 | 4.06 | 3.74 | 1.75 | 0.53 |
| $C_{22}$ | 3.48 | 3.65 | 3.66 | 3.65 | 3.01 | 1.05 | 0.33 |
| $C_{23}$ | 3.06 | 3.22 | 3.23 | 3.20 | 2.34 | 0.73 | 0.25 |
| $C_{24}$ | 2.76 | 2.90 | 2.90 | 2.86 | 1.95 | 0.61 | 0.23 |
| $C_{30}$ | 1.24 | 0.89 | 0.63 | 0.31 | 0.22 | 0.06 | 0.02 |
| $C_{31}$ | 1.01 | 0.55 | 0.33 | 0.11 | 0.08 | 0.02 | 0.00 |
| $C_{32}$ | 0.78 | 0.32 | 0.16 | 0.04 | 0.03 | 0.01 | 0.00 |
| $C_{33}$ | 0.59 | 0.19 | 0.09 | 0.02 | 0.01 | 0.00 | 0.00 |
| $C_{34}$ | 0.46 | 0.12 | 0.06 | 0.01 | 0.01 | 0.00 | 0.00 |
| $C_{35}$ | 0.36 | 0.09 | 0.04 | 0.01 | 0.01 | 0.00 | 0.00 |
| $C_{36}$ | 0.29 | 0.07 | 0.03 | 0.00 | 0.00 | 0.00 | 0.00 |

The fraction of true solid $S$ as well as its composition are then estimated after elimination of the entrapped liquid in residue solid fraction SR:

$$S = \mathrm{SR}(1 - Y) \tag{3}$$

$$X_i^{\mathrm{S}} = \frac{\left(X_i^{\mathrm{SR}} - YX_i^{\mathrm{L}}\right)}{(1 - Y)}. \tag{4}$$

The full experimental characterization of the partially frozen systems (amount and composition) as a function of temperature below the cloud point are reported for each system in Tables 3–7, respectively. Due to experimental uncertainties, these data do not exactly satisfy the mass balance $Z_i = SX_i^S + (1-S)X_i^L$. However, as the differences are within the experimental error, the data were not corrected in order to keep the whole experimental information.

From measurements made in both parts, it is also possible to calculate the amount of crystallization of each heavy paraffin as well as the overall percentage of paraffin crystallized. These data are given in Tables 8–12 and plotted in Fig. 1 which display the overall percentage of paraffin crystallized of each system as a function of temperature. It can be noticed in this figure that, at the beginning of the crystallization, the curvature of the bimodal systems are reversed in comparison to the full series curve. This difference is due to the fact that paraffins continuously crystallize (Fig. 2) in the full series, whereas in bimodal waxes, only the heaviest part precipitate at the beginning of the crystallization (as can be seen on Fig. 3 for mixture *BIM 5*). Thus, the overall percentage of paraffin crystallized rapidly reaches a plateau with most of the heaviest paraffins precipitated. This behavior

Table 6
Experimental characterization of the partially frozen system *BIM 9* as a function of temperature below the onset crystallization temperature

| | 307.15 K | 303.15 K | 298.05 K | 283.25 K | 278.45 K | 273.35 K | 263.05 K |
|---|---|---|---|---|---|---|---|
| *Waxy solid content (mass %)* | | | | | | | |
| | 2.29 | 3.36 | 4.66 | 5.25 | 12.54 | 18.49 | 25.76 |
| *Solid composition (mass %)* | | | | | | | |
| $C_{18}$ | 0.00 | 0.00 | 0.00 | 0.18 | 2.60 | 4.81 | 10.88 |
| $C_{19}$ | 0.00 | 0.00 | 0.00 | 0.16 | 6.59 | 10.65 | 16.82 |
| $C_{20}$ | 0.00 | 0.00 | 0.00 | 0.16 | 11.95 | 16.21 | 18.29 |
| $C_{21}$ | 0.00 | 0.00 | 0.00 | 0.16 | 15.94 | 18.51 | 17.14 |
| $C_{22}$ | 0.00 | 0.00 | 0.00 | 0.18 | 16.81 | 18.04 | 15.45 |
| $C_{32}$ | 14.87 | 16.70 | 19.29 | 23.98 | 11.35 | 7.92 | 5.39 |
| $C_{33}$ | 19.15 | 20.38 | 21.55 | 22.09 | 10.26 | 7.06 | 4.75 |
| $C_{34}$ | 21.76 | 21.74 | 21.33 | 19.80 | 9.14 | 6.27 | 4.22 |
| $C_{35}$ | 22.55 | 21.38 | 19.91 | 17.67 | 8.15 | 5.59 | 3.75 |
| $C_{36}$ | 21.67 | 19.81 | 17.92 | 15.62 | 7.20 | 4.94 | 3.31 |
| *Liquid composition (mass %)* | | | | | | | |
| $C_{10}$ | 68.38 | 69.35 | 69.94 | 70.50 | 76.30 | 80.90 | 90.21 |
| $C_{18}$ | 6.83 | 6.91 | 7.02 | 7.10 | 7.19 | 7.25 | 5.24 |
| $C_{19}$ | 6.22 | 6.29 | 6.39 | 6.47 | 5.95 | 5.19 | 2.34 |
| $C_{20}$ | 5.61 | 5.68 | 5.76 | 5.84 | 4.53 | 3.20 | 1.02 |
| $C_{21}$ | 5.02 | 5.08 | 5.14 | 5.23 | 3.32 | 1.96 | 0.64 |
| $C_{22}$ | 4.52 | 4.57 | 4.63 | 4.70 | 2.65 | 1.46 | 0.56 |
| $C_{32}$ | 1.09 | 0.84 | 0.55 | 0.10 | 0.05 | 0.03 | 0.01 |
| $C_{33}$ | 0.83 | 0.54 | 0.28 | 0.03 | 0.01 | 0.00 | 0.00 |
| $C_{34}$ | 0.63 | 0.34 | 0.14 | 0.01 | 0.00 | 0.00 | 0.00 |
| $C_{35}$ | 0.49 | 0.23 | 0.09 | 0.01 | 0.00 | 0.00 | 0.00 |
| $C_{36}$ | 0.39 | 0.17 | 0.06 | 0.01 | 0.00 | 0.00 | 0.00 |

Table 7
Experimental characterization of the partially frozen system *BIM 13* as a function of temperature below the onset crystallization temperature

| | 308.15 K | 303.15 K | 299.15 K | 279.15 K | 273.15 K | 263.35 K |
|---|---|---|---|---|---|---|
| *Waxy solid content (mass %)* | | | | | | |
| | 1.86 | 2.78 | 4.05 | 4.45 | 15.89 | 26.49 |
| *Solid composition (mass %)* | | | | | | |
| $C_{18}$ | 0.00 | 0.00 | 0.00 | 0.26 | 15.81 | 25.43 |
| $C_{19}$ | 0.00 | 0.00 | 0.00 | 0.22 | 25.64 | 29.60 |
| $C_{20}$ | 0.00 | 0.00 | 0.00 | 0.21 | 28.53 | 27.65 |
| $C_{34}$ | 30.86 | 32.87 | 34.29 | 36.72 | 11.13 | 6.44 |
| $C_{35}$ | 34.94 | 34.59 | 34.28 | 33.23 | 10.03 | 5.78 |
| $C_{36}$ | 34.20 | 32.54 | 31.43 | 29.37 | 8.86 | 5.10 |
| *Liquid composition (mass %)* | | | | | | |
| $C_{10}$ | 68.92 | 69.65 | 70.14 | 71.12 | 80.25 | 91.07 |
| $C_{18}$ | 10.54 | 10.71 | 10.68 | 10.67 | 9.05 | 4.90 |
| $C_{19}$ | 9.57 | 9.72 | 9.75 | 9.60 | 6.14 | 2.30 |
| $C_{20}$ | 8.60 | 8.74 | 8.79 | 8.58 | 4.50 | 1.73 |
| $C_{34}$ | 1.02 | 0.59 | 0.36 | 0.02 | 0.03 | 0.00 |
| $C_{35}$ | 0.76 | 0.35 | 0.18 | 0.00 | 0.02 | 0.00 |
| $C_{36}$ | 0.59 | 0.24 | 0.11 | 0.00 | 0.01 | 0.00 |

Table 8
Percentages of paraffin crystallized as a function of temperature below the onset crystallization temperature for system *BIM 0*

| | 303.15 K | 298.15 K | 293.25 K | 288.05 K | 283.25 K | 273.15 K | 263.15 K |
|---|---|---|---|---|---|---|---|
| Total | 6.59 | 14.87 | 20.71 | 32.72 | 43.16 | 64.16 | 80.93 |
| $C_{18}$ | 0.00 | 0.00 | 0.00 | 0.00 | 0.20 | 4.94 | 24.63 |
| $C_{19}$ | 0.00 | 0.00 | 0.00 | 0.01 | 0.97 | 14.89 | 51.59 |
| $C_{20}$ | 0.00 | 0.00 | 0.00 | 0.51 | 3.47 | 33.23 | 74.85 |
| $C_{21}$ | 0.00 | 0.11 | 0.22 | 2.01 | 9.82 | 54.53 | 86.74 |
| $C_{22}$ | 0.00 | 0.21 | 0.78 | 6.02 | 22.14 | 71.85 | 91.73 |
| $C_{23}$ | 0.00 | 0.37 | 2.34 | 14.49 | 39.20 | 82.45 | 94.33 |
| $C_{24}$ | 0.12 | 0.97 | 6.32 | 28.14 | 56.30 | 88.44 | 96.12 |
| $C_{25}$ | 0.27 | 2.61 | 14.11 | 44.45 | 69.70 | 91.85 | 97.42 |
| $C_{26}$ | 0.75 | 6.49 | 26.18 | 59.62 | 79.02 | 94.22 | 98.31 |
| $C_{27}$ | 2.01 | 13.98 | 40.47 | 71.37 | 85.21 | 95.90 | 98.91 |
| $C_{28}$ | 4.92 | 25.53 | 54.62 | 79.77 | 89.43 | 97.17 | 99.37 |
| $C_{29}$ | 10.35 | 39.82 | 66.56 | 85.68 | 92.44 | 98.08 | 99.55 |
| $C_{30}$ | 18.46 | 53.93 | 75.61 | 89.71 | 94.63 | 98.75 | 99.73 |
| $C_{31}$ | 28.52 | 65.77 | 82.04 | 92.50 | 96.12 | 99.19 | 99.81 |
| $C_{32}$ | 38.98 | 74.50 | 86.31 | 93.56 | 97.15 | 99.41 | 99.85 |
| $C_{33}$ | 47.56 | 79.57 | 88.19 | 94.86 | 97.38 | 99.49 | 100.00 |
| $C_{34}$ | 55.64 | 84.14 | 90.70 | 96.21 | 98.19 | 99.71 | 100.00 |
| $C_{35}$ | 60.84 | 86.33 | 91.45 | 96.54 | 98.42 | 99.81 | 100.00 |
| $C_{36}$ | 64.44 | 87.68 | 91.98 | 96.91 | 98.56 | 99.76 | 100.00 |

Table 9
Percentages of paraffin crystallized as a function of temperature below the onset crystallization temperature for system *BIM 3*

| | 305.15 K | 301.15 K | 296.05 K | 278.35 K | 273.15 K | 263.15 K |
|---|---|---|---|---|---|---|
| Total | 6.87 | 11.56 | 15.49 | 46.57 | 61.51 | 78.84 |
| Lightest part | 0.00 | 0.00 | 0.11 | 33.04 | 50.78 | 73.00 |
| Heaviest part | 30.75 | 51.60 | 70.60 | 97.02 | 98.95 | 99.59 |
| $C_{18}$ | 0.00 | 0.00 | 0.00 | 2.14 | 7.12 | 27.49 |
| $C_{19}$ | 0.00 | 0.00 | 0.00 | 6.45 | 19.29 | 55.08 |
| $C_{20}$ | 0.00 | 0.00 | 0.00 | 16.63 | 39.37 | 77.10 |
| $C_{21}$ | 0.00 | 0.00 | 0.00 | 32.99 | 60.63 | 87.90 |
| $C_{22}$ | 0.00 | 0.00 | 0.00 | 50.87 | 75.84 | 92.53 |
| $C_{23}$ | 0.00 | 0.00 | 0.00 | 65.05 | 83.78 | 94.41 |
| $C_{24}$ | 0.00 | 0.00 | 0.47 | 73.11 | 87.23 | 95.23 |
| $C_{25}$ | 0.00 | 0.00 | 0.84 | 77.17 | 88.90 | 95.67 |
| $C_{29}$ | 7.10 | 17.41 | 36.73 | 91.38 | 95.99 | 98.81 |
| $C_{30}$ | 13.91 | 30.67 | 55.56 | 95.52 | 98.06 | 99.45 |
| $C_{31}$ | 23.12 | 45.59 | 71.13 | 97.81 | 100.00 | 100.00 |
| $C_{32}$ | 33.35 | 59.14 | 81.34 | 98.90 | 100.00 | 100.00 |
| $C_{33}$ | 42.92 | 69.30 | 87.08 | 99.26 | 100.00 | 100.00 |
| $C_{34}$ | 50.47 | 76.19 | 90.09 | 99.48 | 100.00 | 100.00 |
| $C_{35}$ | 55.81 | 80.59 | 91.58 | 99.57 | 100.00 | 100.00 |
| $C_{36}$ | 59.43 | 83.10 | 92.23 | 99.61 | 100.00 | 100.00 |

Table 10
Percentages of paraffin crystallized as a function of temperature below the onset crystallization temperature for system *BIM 5*

| | 306.15 K | 298.15 K | 294.15 K | 286.25 K | 283.35 K | 273.45 K | 263.35 K |
|---|---|---|---|---|---|---|---|
| Total | 6.82 | 13.24 | 15.87 | 19.36 | 29.32 | 58.81 | 79.04 |
| Lightest part | 0.00 | 0.00 | 0.00 | 0.81 | 12.72 | 48.65 | 73.74 |
| Heaviest part | 33.23 | 68.06 | 80.91 | 93.12 | 95.36 | 98.97 | 99.77 |
| $C_{18}$ | 0.00 | 0.00 | 0.00 | 0.03 | 0.42 | 7.99 | 31.76 |
| $C_{19}$ | 0.00 | 0.00 | 0.00 | 0.08 | 1.53 | 22.49 | 60.92 |
| $C_{20}$ | 0.00 | 0.00 | 0.00 | 0.23 | 4.85 | 44.28 | 81.44 |
| $C_{21}$ | 0.00 | 0.00 | 0.00 | 0.60 | 11.90 | 64.26 | 90.04 |
| $C_{22}$ | 0.00 | 0.00 | 0.00 | 1.28 | 21.92 | 76.36 | 93.15 |
| $C_{23}$ | 0.00 | 0.00 | 0.00 | 2.08 | 31.21 | 81.53 | 94.03 |
| $C_{24}$ | 0.00 | 0.00 | 0.00 | 2.76 | 36.25 | 82.69 | 93.89 |
| $C_{30}$ | 11.01 | 37.29 | 55.76 | 78.62 | 85.45 | 96.54 | 99.23 |
| $C_{31}$ | 19.66 | 55.72 | 73.82 | 91.38 | 94.38 | 98.91 | 99.77 |
| $C_{32}$ | 29.82 | 70.72 | 85.05 | 96.47 | 97.69 | 99.57 | 99.91 |
| $C_{33}$ | 39.69 | 80.37 | 90.78 | 98.23 | 98.82 | 99.76 | 99.95 |
| $C_{34}$ | 47.79 | 85.71 | 93.36 | 98.95 | 99.23 | 99.82 | 99.96 |
| $C_{35}$ | 53.60 | 88.47 | 94.55 | 99.20 | 99.39 | 99.84 | 99.96 |
| $C_{36}$ | 57.52 | 89.89 | 95.14 | 99.30 | 99.44 | 99.88 | 99.97 |

Table 11
Percentages of paraffin crystallized as a function of temperature below the onset crystallization temperature for system *BIM 9*

| | 307.15 K | 303.15 K | 298.05 K | 283.25 K | 278.45 K | 273.35 K | 263.05 K |
|---|---|---|---|---|---|---|---|
| Total | 6.90 | 10.18 | 13.98 | 15.82 | 37.70 | 54.30 | 77.99 |
| Lightest part | 0.00 | 0.00 | 0.00 | 0.16 | 24.64 | 44.81 | 73.59 |
| Heaviest part | 40.66 | 61.98 | 81.32 | 97.45 | 99.05 | 99.52 | 99.90 |
| $C_{18}$ | 0.00 | 0.00 | 0.00 | 0.14 | 4.93 | 13.10 | 41.88 |
| $C_{19}$ | 0.00 | 0.00 | 0.00 | 0.14 | 13.72 | 31.76 | 71.40 |
| $C_{20}$ | 0.00 | 0.00 | 0.00 | 0.15 | 27.46 | 53.47 | 86.18 |
| $C_{21}$ | 0.00 | 0.00 | 0.00 | 0.17 | 40.76 | 68.12 | 90.35 |
| $C_{22}$ | 0.00 | 0.00 | 0.00 | 0.21 | 47.67 | 73.73 | 90.60 |
| $C_{32}$ | 24.20 | 40.72 | 62.98 | 93.31 | 97.11 | 98.53 | 99.70 |
| $C_{33}$ | 35.21 | 56.84 | 79.10 | 97.95 | 99.35 | 99.69 | 99.92 |
| $C_{34}$ | 44.89 | 68.69 | 87.80 | 99.04 | 99.76 | 99.89 | 99.95 |
| $C_{35}$ | 52.07 | 76.10 | 91.88 | 99.29 | 99.89 | 99.93 | 100.00 |
| $C_{36}$ | 56.58 | 80.02 | 93.63 | 99.37 | 99.92 | 99.94 | 100.00 |

can also be noticed in Fig. 4 in which distribution of paraffins within the solid part is represented schematically for system *BIM 9*.

## 3. Thermodynamic modelling

Solid–liquid equilibrium can be described by an equation relating the composition of component *i* in the solid and liquid phases with their nonideality and the thermophysical properties of pure components [9]:

$$\ln\frac{x_i^{\mathrm{S}}\gamma_i^{\mathrm{S}}}{x_i^{\mathrm{L}}\gamma_i^{\mathrm{L}}} = \frac{\Delta h_{\mathrm{m}}}{RT_{\mathrm{m}}}\left[\frac{T_{\mathrm{m}}}{T}-1\right] + \frac{\Delta h_{\mathrm{tr}}}{RT_{\mathrm{tr}}}\left[\frac{T_{\mathrm{tr}}}{T}-1\right]. \tag{5}$$

The heats and temperatures of phase transition are obtained from literature values [10] for the *n*-alkanes with an odd carbon number chain length. Since it is assumed that the solid phase is

Table 12
Percentages of paraffin crystallized as a function of temperature below the onset crystallization temperature for system *BIM 13*

| | 308.15 K | 303.15 K | 299.15 K | 279.15 K | 273.15 K | 263.35 K |
|---|---|---|---|---|---|---|
| Total | 5.74 | 8.60 | 12.38 | 13.89 | 48.88 | 80.15 |
| Lightest part | 0.00 | 0.00 | 0.00 | 0.11 | 40.15 | 76.95 |
| Heaviest part | 44.38 | 70.72 | 86.74 | 99.41 | 99.03 | 100.00 |
| $C_{18}$ | 0.00 | 0.00 | 0.00 | 0.11 | 24.81 | 65.18 |
| $C_{19}$ | 0.00 | 0.00 | 0.00 | 0.11 | 44.08 | 82.28 |
| $C_{20}$ | 0.00 | 0.00 | 0.00 | 0.11 | 54.47 | 85.18 |
| $C_{34}$ | 36.32 | 61.30 | 80.10 | 98.79 | 98.77 | 100.00 |
| $C_{35}$ | 46.66 | 73.68 | 89.09 | 99.70 | 99.16 | 100.00 |
| $C_{36}$ | 52.25 | 79.69 | 92.45 | 99.86 | 99.22 | 100.00 |

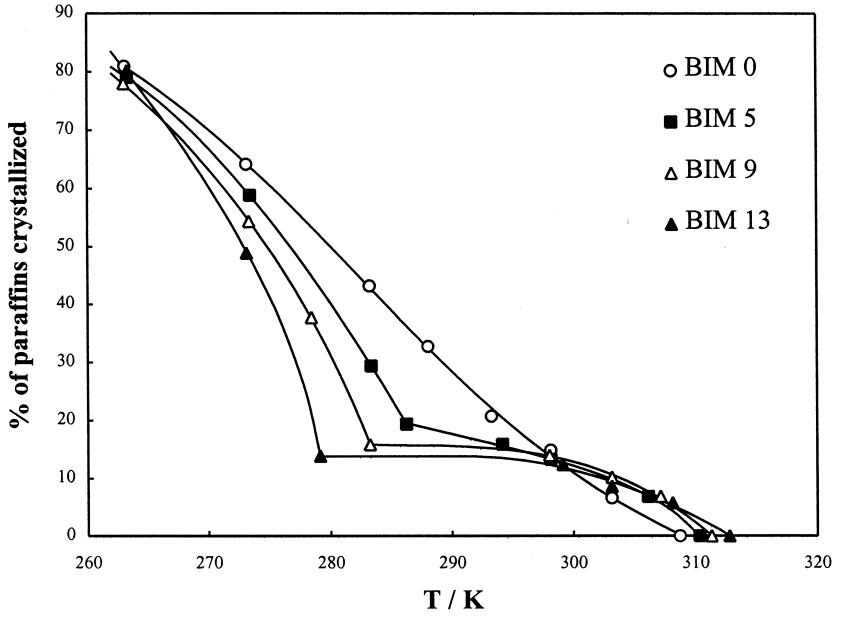


Fig. 1. Overall percentage of paraffins crystallized vs. temperature.

orthorhombic, the properties for the even-numbered chain length paraffins are obtained by interpolating the values for the odd-numbered alkanes. From Eq. (5), the composition and the size of the phases in equilibrium can be calculated if a model for the nonideality of the phases is available.

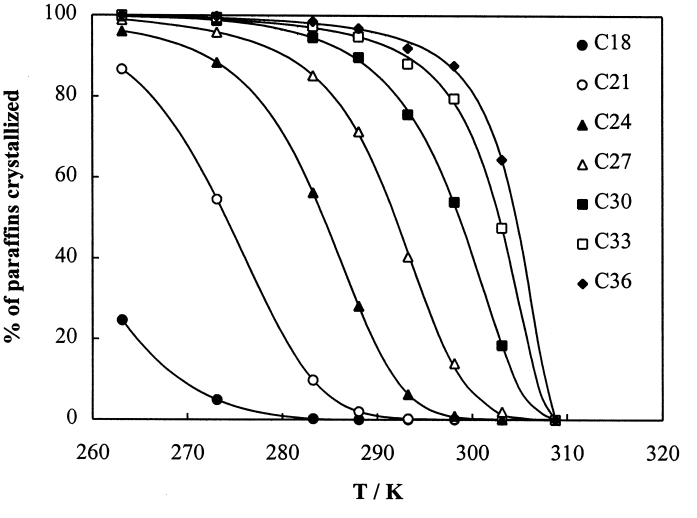


Fig. 2. Percentage of paraffins crystallized vs. temperature and carbon number for mixture *BIM 0*.

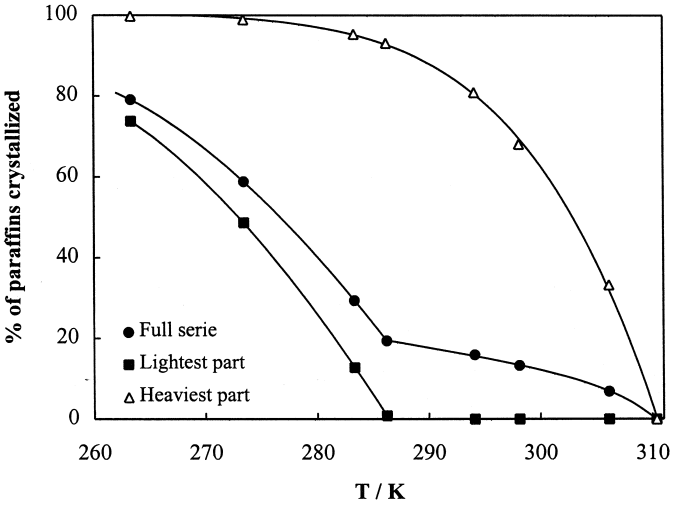


Fig. 3. Percentage of paraffins crystallized as a function of temperature for each part of the bimodal distribution *BIM 5*.

For the liquid phase nonideality, the Flory-free volume model will be used, in accordance with the results of a previous work [2], to take into account the combinatorial and free volume effects that arise due to the size difference between the molecules:

$$\ln \gamma_i^{\text{comb-fv}} = \ln\frac{\phi_i}{x_i} + 1 - \frac{\phi_i}{x_i} \tag{6}$$

with

$$\phi_i = \frac{x_i\left(V_i^{1/3} - V_{wi}^{1/3}\right)^{3.3}}{\sum_j x_j\left(V_j^{1/3} - V_{wj}^{1/3}\right)^{3.3}}. \tag{7}$$

The solid phase nonideality will be described by two well-known local composition models, Wilson [4] and UNIQUAC [7] which allows multi-solid phase equilibrium calculation. The Wilson equation used in this work can be written as

$$\frac{g^E}{RT} = -\sum_{i=1}^{m} x_i \ln\left[\sum_{j=1}^{m} x_j \exp\left(-\frac{\lambda_{ij} - \lambda_{ii}}{RT}\right)\right] \tag{8}$$

and the version of the UNIQUAC model used is

$$\frac{g^E}{RT} = \sum_{i=1}^{n} x_i \ln\left(\frac{\Phi_i}{x_i}\right) + \frac{Z}{2}\sum_{i=1}^{n} q_i x_i \ln\frac{\theta_i}{\Phi_i} - \sum_{i=1}^{n} x_i q_i \ln\left[\sum_{j=1}^{n} \theta_j \exp\left(-\frac{\lambda_{ij} - \lambda_{ii}}{q_i RT}\right)\right] \tag{9}$$

with

$$\Phi_i = \frac{x_i r_i}{\sum_j x_j r_j} \quad \text{and} \quad \theta_i = \frac{x_i q_i}{\sum_j x_j q_j} \tag{10}$$

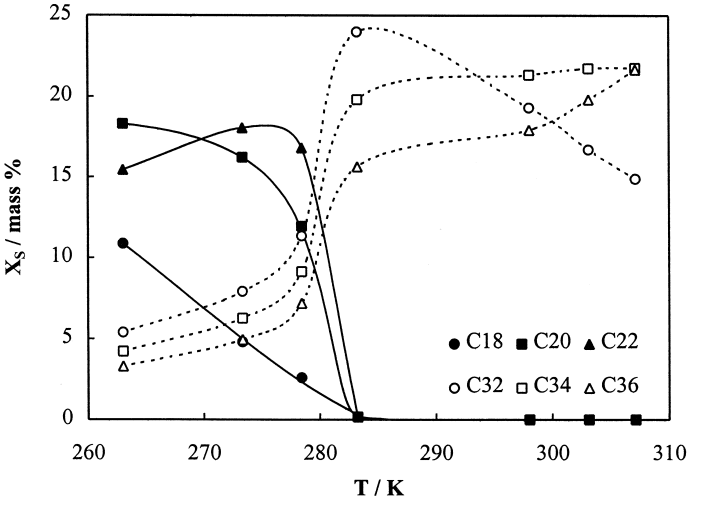


Fig. 4. Wax composition (mass %) vs. temperature for system *BIM 13*.

and using structural parameters $r$ and $q$ estimated [6] to take into account the specificity of the interactions in the solid phase:

$$r_i = \frac{r_{i\text{org}}}{6.744} \quad \text{and} \quad q_i = \frac{q_{i\text{org}}}{5.40}. \tag{11}$$

The predictive local composition concept [3] allows an 'a priori' estimation of the interaction energies, $\lambda_{ij}$, used by these models. The pair interaction energies between two identical molecules are estimated from the heat of sublimation of an orthorhombic crystal of the pure component

$$\lambda_{ii} = -\frac{2}{Z}\left(\Delta h_{\text{sblm}_i} - RT\right), \tag{12}$$

with $Z$ being the coordination number, considered to be 6 for the orthorhombic crystal. The heats of sublimation, $h_{\text{sblm}} = h_{\text{vap}} + h_{\text{m}} + h_{\text{tr}}$, are calculated at the melting temperature of the pure component. The heat of vaporisation $h_{\text{vap}}$ is assessed using a correlation by Morgan and Kobayashi [11]. The pair interaction energy $\lambda_{ij}$ between a long and a short molecule is related to the contact area between the molecules which is assumed [3] identical to the contact area between two short molecules; thus,

$$\lambda_{ij} = \lambda_{jj}, \tag{13}$$

where $j$ is the *n*-alkane with the shorter chain of the pair $ij$. The Solid–Liquid equilibrium model is thus a purely predictive model that uses in the calculation of the phase behaviour only pure component properties.

## 4. Results and discussion

Table 2 displays deviations between experimental onset crystallisation temperatures and model cloud point predictions using Wilson equation or UNIQUAC for describing solid phase nonideality in

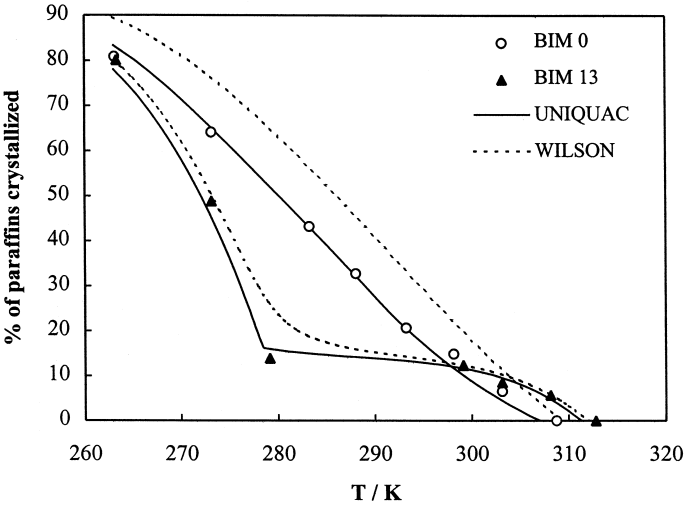


Fig. 5. Comparison between experimental and calculated overall percentage of paraffins crystallized.

model. On reading this table, one can observe, as for previous systems [5], that the use of Wilson equation provides a satisfactory description of the wax appearance temperatures with deviations less than experimental error. Use of UNIQUAC equation leads to an underestimation of about 2 K of the onset crystallisation temperature which means that UNIQUAC overestimate the nonideality of the solid solution at the beginning of the crystallisation. However, as it can be seen on Figs. 5 and 6, which represents the percentage of paraffins crystallized for *BIM 0* and *BIM 13* and the composition of the waxy solid vs. temperature for *BIM 5*, UNIQUAC improves the description of bimodal systems. In particular, the break points, which are linked to the onset crystallization of the lightest part of the heavy fraction, are well-reproduced by the model. This improvement, compared with Wilson

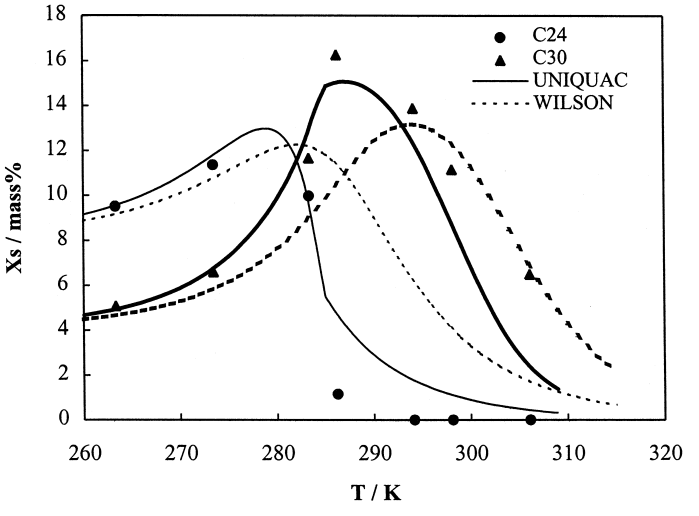


Fig. 6. Composition of C24 and C30 in solid wax calculated using either Wilson equation or UNIQUAC for system *BIM 5*.

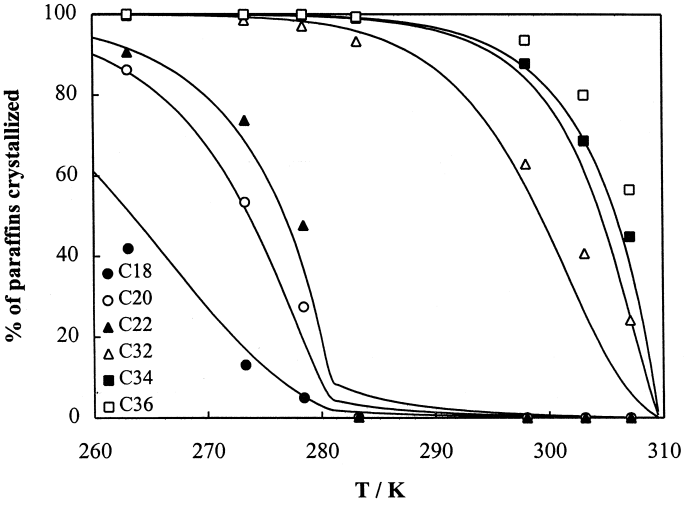


Fig. 7. Amount of crystallization calculated using UNIQUAC for several paraffins in *BIM 9*.

equation, is no doubt connected with the fact that UNIQUAC allows solid–solid phase equilibrium calculation. The percentages of crystallization corresponding to the individual paraffins were also plotted as a function of temperature for system *BIM 9* (Fig. 7) in order to demonstrate the predictive capacity of the model using UNIQUAC. It can be verified that the calculated curves fit extremely well with the experimental points. Shapes and break points are well-reproduced by the model. This performance, which is achieved without adjustments of parameters, shows that the model provides a good description of the thermodynamic mechanism of crystallization as a function of temperature. In particular, use of UNIQUAC instead of Wilson equation clearly improves the representation of light

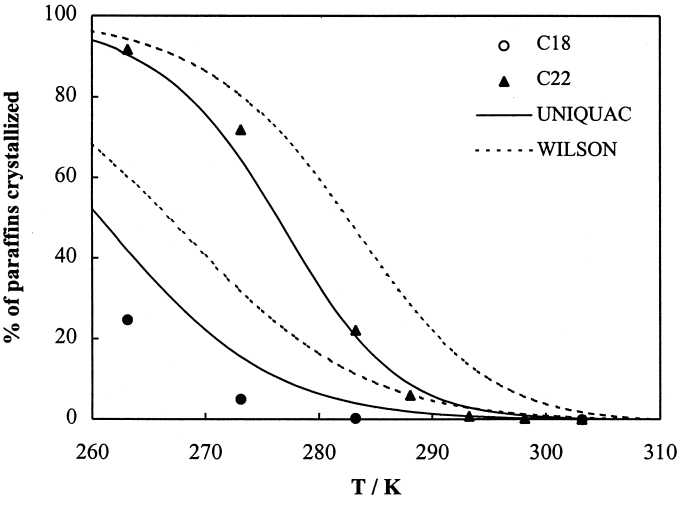


Fig. 8. Percentage of crystallization of lightest components in mixture *BIM 0* calculated using either Wilson equation or UNIQUAC.

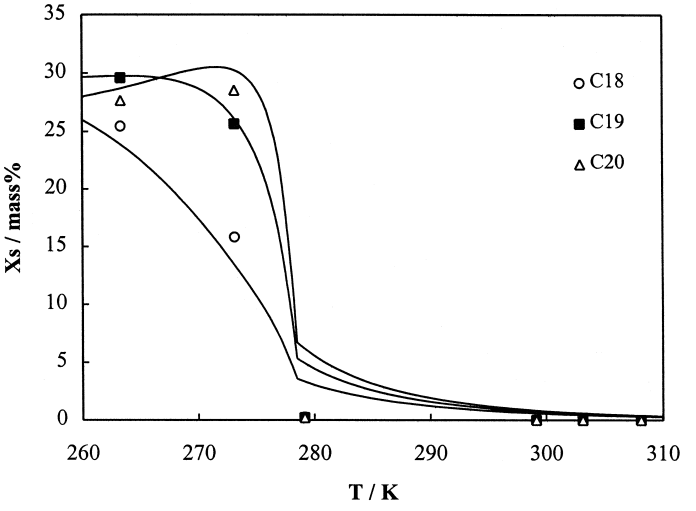


Fig. 9. Composition of the lightest components in solid wax calculated using UNIQUAC for *BIM 13*.

paraffins content (i.e., Fig. 8 for *BIM 0*). Nevertheless, as it can be observed on Fig. 9 for mixture *BIM 13*, the model still predicts the presence (in small proportion) of light paraffins in solid just below the melting temperature, whereas they were experimentally not found.

## 5. List of symbols

| | |
|---|---|
| $g$ | Gibbs energy |
| $h$ | enthalpy |
| $R$ | ideal gas constant |
| $T$ | temperature |
| $V$ | volume |
| $q$ | area parameter (UNIQUAC) |
| $r$ | volume parameter (UNIQUAC) |
| $S$ | mass fraction of solid in partially frozen system |
| SR | mass fraction of solid residue of filtration |
| $x_i$ | mole fraction of i |
| $X_i$ | mass fraction of i |
| $Y$ | mass fraction of trapped liquid in the solid residue of filtration |
| $Z$ | coordination number |
| *Greek letters* | |
| $\alpha$ | distribution coefficient |
| $\gamma$ | activity coefficient |
| $\phi$ | volume fraction |
| $\lambda$ | interaction parameter |
| $\theta$ | area fraction |

*Superscripts*

| | |
|---|---|
| comb | combinatorial |
| E | excess |
| fv | free volume |
| L | liquid |
| S | solid |
| SR | solid residue |

*Subscripts*

| | |
|---|---|
| *i* | component |
| m | melting |
| *n* | carbon number |
| tr | solid–solid transition |
| sblm | sublimation |
| vap | vaporization |
| w | Van der Waals |

## References

[1] J.A.P. Coutinho, V. Ruffier-Mèray, Ind. Eng. Chem. Res. 36 (1997) 4977.
[2] J.A.P. Coutinho, S.I. Andersen, E.H. Stenby, Fluid Phase Equilibria 103 (1995) 23.
[3] J.A.P. Coutinho, K. Knudsen, S.I. Andersen, E.H. Stenby, Chem. Eng. Sci. 51 (1996) 3273.
[4] G.M. Wilson, J. Am. Chem. Soc. 86 (1964) 127.
[5] J. Pauly, C. Dauphin, J.L. Daridon, Fluid Phase Equilibria 149 (1998) 191.
[6] J.A.P. Coutinho, Ind. Eng. Chem. Res. 37 (1998) 4870.
[7] D.S. Abrams, J.M. Prausnitz, AIChE J. 21 (1975) 116.
[8] Daridon, P. Xans, F. Montel, Fluid Phase Equilibria 117 (1996) 241.
[9] J.M. Prausnitz, Molecular Thermodynamics of Fluid Phase Equilibria, Prentice-Hall, Englewood Cliffs, NJ, 1969.
[10] M.G. Broadhurst, J. Res. Nat. Bur. Stand. 66 (1962) 241.
[11] D.L. Morgan, R. Kobayashi, Fluid Phase Equilibria 94 (1994) 51.